applied optics

Exact surface profile measurement without subtracting dispersion phase through Fourier transform in a white-light scanning interferometer

Songjie Luo,[1,2] Osami Sasaki,[1,2] Ziyang Chen,[1] Samuel Choi,[2] and Jixiong Pu[1,*]

[1]Fujian Provincial Key Laboratory of Light Propagation and Transformation, College of Information Science and Engineering, Huaqiao University, Xiamen, Fujian 361021, China
[2]Faculty of Engineering, Niigata University, Niigata 950-2181, Japan
*Corresponding author: jixiong@hqu.edu.cn

Received 19 October 2017; revised 3 January 2018; accepted 3 January 2018; posted 5 January 2018 (Doc. ID 309104); published 31 January 2018

A new signal processing is proposed in which the dispersion phase is not subtracted from the detected spectral phase distribution. The linear and bias components in the spectral phase distribution are used to calculate the complex-valued interference signal (CVIS). The simulations verify that the dispersion phase generates an inclination in the measured surface profile along one direction in which the magnitude of the dispersion phase changes linearly. The simulations also show that the position of zero phase nearest the position of amplitude maximum in the CVIS almost does not change due to the bias component, although the random phase noise contained in the interference signal changes the slope of the linear component. Measured surface profiles show that the new signal processing achieves highly accurate measurement by the CVIS.

OCIS codes: (120.3180) Interferometry; (120.4825) Optical time domain reflectometry; (120.5050) Phase measurement.

https://doi.org/10.1364/AO.57.000894

1. INTRODUCTION

White-light scanning interferometers (WLSIs) have been used to measure three-dimensional shapes of reflecting surfaces since early times. If measurement error in WLSIs is less than several nanometers, a WLSI is a very powerful tool that has a wide measurement region with a measurement accuracy of nanometer order. In order to achieve high measurement accuracy, different techniques to determine a position of a reflecting surface from the interference signal have been proposed. Detected interference signals have two important positions along the scanning position. One is the maximum value of the envelope, which is called envelope peak [1,2], coherence peak [3], or top of envelope [4]. The other is the maximum value of the interference signal, which is called fringe peak [1], phase peak [2], or signal maximum [4]. It has been reported that the fringe peak provides better accuracy in position measurement compared with the envelope peak [1,2,4]. Although the fringe peak is strongly related to the position where the phase of the interference signal is zero, the position of the fringe peak is not exactly the same as the position of zero phase because the interference signal is a product of the coherence function and the cosine function of the phase distribution. Therefore, it is important to obtain exactly the position of zero phase nearest to the envelope peak. The phase-shifting method [3] and the lock-in evaluation method [5] were used to obtain the position of zero phase nearest to the envelope peak. These two methods focus on the waveform of the real-valued interference signal itself. On the other hand, Fourier transform of the real-valued interference signal or spectral distribution in wavenumber domain contains useful information about the interference signal [2,6–8]. When there is no dispersion effect and no noise effect in the interference signal, a magnitude of nonlinear component in the spectral phase distribution is very small. The position of the reflecting surface has been obtained from the slope of the linear component in the spectral phase distribution [6,7]. In order to utilize information about amplitude and phase, the complex-valued interference signal (CVIS) is calculated by Fourier transform of the positive components of the spectral distribution [8]. The position of zero phase nearest to the position of amplitude maximum can be easily obtained, and its position provides an accurate measurement of surface profile. In Ref. [8] the dispersion phase was exactly eliminated in the spectral phase distribution to get highly accurate measurement.

In this paper, a new signal processing is proposed in which the dispersion phase is not subtracted from the detected spectral phase distribution. A least squares line is calculated in the spectral phase distribution, and the linear and bias components in the spectral phase distribution are used to calculate the CVIS.

How the dispersion phase provides effects on the linear and bias components when a random phase noise exists in the interference signal is examined by simulations. The simulations verify that the dispersion phase generates an inclination in the measured surface profile along one direction in which the magnitude of the dispersion phase changes linearly. The simulations also show the random phase noise changes the slope of the linear component, but the position of zero phase nearest to the position of amplitude maximum in the CVIS almost does not change due to the bias component. These characteristics lead to highly accurate measurement by the new signal processing without using the dispersion phase measured with a spectrally resolved interferometer.

2. PRINCIPLE

Figure 1 shows a WLSI with a supercontinuum light source whose spectral intensity is $I(\sigma)$, where σ is the wavenumber. The position of an object surface is z_o, and the position z of a reference surface is scanned by a piezoelectric transducer (PZT). An interference signal is detected with a camera when the PZT is moving. The interference signal expressed as a function of the scanning position z is given by

$$S(z) = \int_{-\infty}^{\infty} I(\sigma)\cos[4\pi(z - z_o)\sigma + \varphi_n(z)\sigma + \varphi_d(\sigma)]\mathrm{d}\sigma, \tag{1}$$

where phase $\varphi_d(\sigma)$ is a dispersion phase caused by two sides of unequal length in a cubic beam splitter. The two beams reflected from the object surface and the reference surface have path distances of l_1 and l_2 in the beam splitter, respectively, as shown in Fig. 2. Denoting the distance difference by $l_\varepsilon = l_1 - l_2$, the dispersion phase is given by

$$\varphi_d(\sigma) = 4\pi[n(\sigma) - 1]\sigma l_\varepsilon, \tag{2}$$

where $n(\sigma)$ is the refractive index of the beam splitter, and l_ε is a linear function of the position x where the two beams go out from the beam splitter. At $x = x_B$, the value of l_ε is almost equal to zero, and it increases linearly as the position x approaches x_A, as shown in Fig. 2. Phase $\varphi_n(z)$ is generated by an optical path change that is caused by random disturbances such as mechanical vibrations and non-constant speed of the PZT movement. Fourier transform of $S(z)$ or the

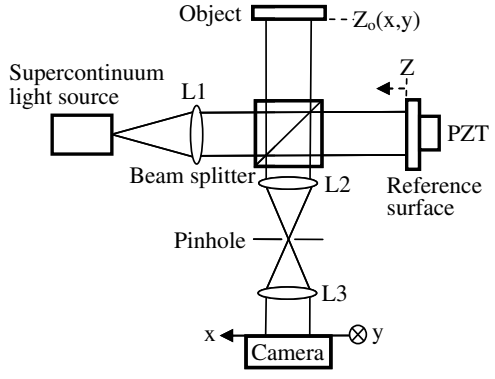

Fig. 1. Schematic of a white-light scanning interferometer.

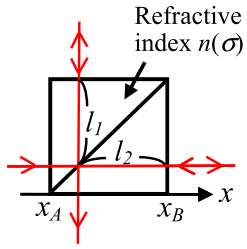

Fig. 2. Generation of dispersion phase by the distance difference of $l_\varepsilon = l_1 - l_2$ in the beam splitter.

spectral distribution in the region of positive wavenumbers is expressed as

$$F(\sigma) = I_F(\sigma)e^{-j4\pi z_o\sigma}e^{j\beta(\sigma)}, \qquad (\sigma > 0), \tag{3}$$

where $\beta(\sigma)$ arises from the phases $\varphi_n(z)\sigma$ and $\varphi_d(\sigma)$ through Fourier transform. Denoting the least squares line in the phase distribution of Eq. (3) by $a_0 + (a_1 - 4\pi z_0)\sigma$, a new spectral distribution having only bias and linear phases is obtained as

$$F_L(\sigma) = I_F(\sigma)e^{j(a_1 - 4\pi z_o)\sigma}e^{ja_o}, \qquad (\sigma > 0). \tag{4}$$

Since the phase distribution of Eq. (3) is unwrapped to calculate the least squares line, the value of a_0 is more than 2π. Expressing the inverse Fourier transform of $I_F(\sigma)$ by $A(2z)e^{j\alpha(2z)}$, the CVIS derived as inverse Fourier transform of $F_L(\sigma)$ is given by

$$S_c(z) = A(z - z_s)\exp[j\alpha(z - z_s) + ja_0], \tag{5}$$

where $z_s = z_0 - (a_1/4\pi)$, $A(z) = A(-z)$, $\alpha(z) = -\alpha(z)$, and $\alpha(0) = 0$. The period of the phase distribution in the CVIS is $\lambda_A/2$ around $z = z_s$, where λ_A is the weighted average wavelength in the distribution of $I_F(\sigma)$. The value of a_0 in Eq. (5) exists in the range from $-\pi$ to π after the value of a_0 in Eq. (4) is reduced to $a_0 - 2\pi n$, where n is an integer. Equation (5) leads to the following results: a position z_a of maximum amplitude of $A(z - z_s)$ is equal to the measurement value z_s obtained from the slope of the linear component in the spectral phase. The position z_p of zero phase nearest to the position z_a is given by

$$z_p = z_s + (a_0\lambda_A/4\pi) = z_0 - (a_1/4\pi) + (a_0\lambda_A/4\pi). \tag{6}$$

The following characteristics are estimated: the existence of the dispersion phase produces an inclination of a surface profile in the direction of x axis, because it is expected that the distance difference l_ε in the dispersion phase $\varphi_d(\sigma)$ changes linearly along the x axis, and the values of a_1 and a_0 increase linearly with increase in the value of l_ε. The existence of the noise phase $\varphi_n(z)$ does not generate a large measurement error in the measurement value z_p, because the value of a_0 caused by $\varphi_n(z)$ will compensate for a change in a_1 caused by $\varphi_n(z)$. These characteristics are verified by simulations and experiments in the following sections.

3. SIMULATION

First, it will be explained how the simulation is carried out following the principle. In order to generate the interference signal given by Eq. (1), the spectrum $I(\sigma)$, the phase distributions $\varphi_d(\sigma)$, and the random phase noise $\varphi_n(z)$ are necessary. Figure 3 shows the spectrum of the supercontinuum light

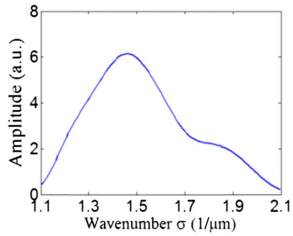

Fig. 3. Spectrum $I(\sigma)$ of the light source.

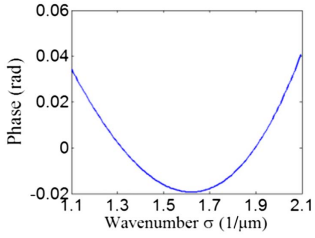

Fig. 4. Nonlinear component contained in $4\pi[n(\sigma) - 1]\sigma$.

source, which was detected by a spectral analyzer [8]. The wavenumber region of the detected spectrum was from 1.1 to 2.1 μm^{-1}. The difference between the lengths of the two sides of the beam splitter was about 100 μm. The nonlinear component contained in the dispersion phase $\varphi_d(\sigma)$ at $l_\varepsilon =$ 1 μm was calculated with least squares method, as shown in Fig. 4. The dispersion phase $\varphi_d(\sigma)$ of $l_\varepsilon = 40$ μm around the central position of the beam splitter was used. Figure 5 is the random Gaussian noise $\varphi_n(z)$ with an average of zero and variance of 0.09 rad · μm. The interference signal was generated in the region from −30 μm to 30 μm where the object position z_o was 1 μm, and the sampling interval Δz and the sampling number N were 0.0073 μm and 8192, respectively. A part of interference signal whose envelope value was more than one-tenth of its maximum intensity was selected by a rectangular window whose width was from −23 μm to −18 μm, as shown in Fig. 6. The other data outside the rectangular window were zero values. Fourier transform was performed on this interference signal of data number N. The interval of wavenumber was $\Delta\sigma = 1/(2N\Delta z) = 0.0083$ μm^{-1}. Figure 7(a) show the amplitude $I_F(\sigma)$ of Fourier transform $F(\sigma)$. The values of a_0 and $a_1 - 4\pi z_o$ were −280.721 rad and 257.486 rad · μm, respectively. The phase distribution of $F(\sigma)$ contained a large value of a_1 of 270.053 rad · μm, which was almost caused by

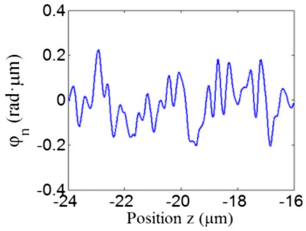

Fig. 5. Gaussian noise with average of zero and variance of 0.09 rad · μm.

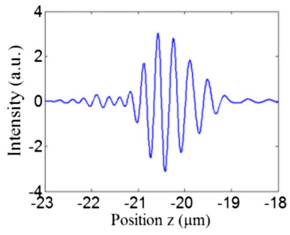

Fig. 6. Interference signal generated with the spectrum, the dispersion phase, and the Gaussian noise.

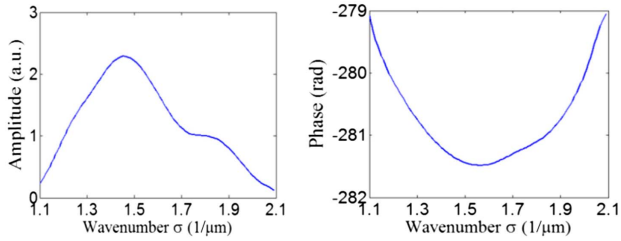

Fig. 7. Fourier transform of the interference signal of Fig. 6; (a) amplitude $I_F(\sigma)$ and (b) phase of $\beta(\sigma) - a_1\sigma$.

the dispersion phase at $l_\varepsilon = 40$ μm. In order to show clearly the non-linear component contained in the phase of $F(\sigma)$, the phase distribution of $\beta(\sigma) - a_1\sigma$ is shown in Fig. 7(b), where the a_0 was equal to −280.721 rad · μm. The measurement value z_s of the object position was obtained from the linear component of the phase distribution as $z_s = z_o - a_1/4\pi = -20.490$ μm. By performing inverse Fourier transform on the data of $F_L(\sigma)$, the CVIS was obtained as shown in Figs. 8(a) and 8(b). The value of z_a was −20.490 μm, which was equal to z_s. The measurement value z_p of the object position obtained from this CVIS was −20.596 μm.

Second, in order to examine the effect of the dispersion phase, the different values of l_ε were used in the simulation when the noise φ_n did not exist. Results are shown in Table 1. The values of a_o and a_1 change linearly with the increase of l_ε. The interval in a_o and a_1 between the adjacent values of l_ε were constant by ignoring small fluctuations less than 5 nm and 3 rad · μm, respectively. The average values of the interval in a_o and a_1 were about 73.470 rad and 67.604 rad · μm, respectively. The values $z_s - z_o$ and $z_p - z_o$

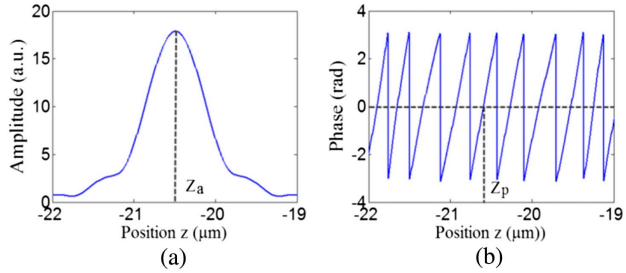

Fig. 8. Complex-valued interference signal of Fig. 6 obtained by using the least squares line.

Table 1. Simulation Results at the Different Values of l_ε Without Noise

l_ε (μm)	0	10	20	30	40
a_0 (rad)	12.566	−60.903	−134.371	−207.841	−281.312
a_1 (rad · μm)	0.0	67.604	135.206	202.811	270.415
$z_s - z_o$ (μm)	0.0	−5.380	−10.759	−16.139	−21.519
$z_p - z_o$ (μm)	0.0	−5.481	−10.633	−16.113	−21.594

were obtained from the CVIS. These two values almost satisfied Eq. (6). The decreasing interval in the values of $z_s - z_o$ between adjacent values of l_ε was a constant value of 5.380 μm by ignoring fluctuations less than 1 nm. On the other hand, the interval of 5.152 μm in the values of $z_p - z_o$ between $l_\varepsilon = 10$ μm and $l_\varepsilon = 20$ μm is not equal to the constant interval of 5.481 μm between the other adjacent values of l_ε. After adding a value of $\lambda_A/2 = 0.329$ μm to the values of $z_p - z_o$ at $l_\varepsilon = 20$ μm, 30 μm, and 40 μm, all the intervals in $z_p - z_o$ between the adjacent values became the constant value of 5.481 μm. It is made clear from the results in Table 1 that the dispersion phase brings only an inclination along the x axis to a measured surface profile. Therefore, the dispersion phase has no influence on the measurement accuracy.

Third, the simulation was carried out when the dispersion and noise existed together. The simulation results are shown at Table 2. Although all the values are different from the results in Table 1, the values of $z_s - z_o$ and $z_p - z_o$ also satisfy Eq. (6). Due to the effect of noise, the interval in the values of $z_s - z_o$ between the adjacent values of l_ε was not constant, and the deviations from the average value of 5.369 μm were less than 60 nm. The interval of 5.151 μm in the values of $z_p - z_o$ between $l_\varepsilon = 10$ μm and $l_\varepsilon = 20$ μm was not equal to the constant interval of 5.482 μm between the other adjacent values of l_ε. After adding a value of $\lambda_A/2 = 0.329$ μm to the values of $z_p - z_o$ at $l_\varepsilon = 20$ μm, 30 μm, and 40 μm, all the intervals in $z_p - z_o$ became almost constant, and the deviation from the average value of 5.482 μm was less than 4 nm. Therefore, the noise has a large influence on the linear change in the values of $z_s - z_o$, compared with the values of $z_p - z_o$.

In order to show degree of noise resistance, the values of $z_s - z_o$ and $z_p - z_o$ were compared between Tables 1 and 2. The differences of the values are denoted by $\Delta(z_s - z_o)$ and $\Delta(z_p - z_o)$ in Table 3. The $\Delta(z_p - z_o)$ and $\Delta(z_s - z_o)$ are less than 3 nm and 39 nm, respectively. These results make clear that the value z_p has a higher noise resistance and provides higher accuracy in surface profile measurement.

Finally, the simulation was carried out for different noises at $l_\varepsilon = 40$ μm, as shown in Table 4. Noise I was used in Table 2. The averages and variances of 3 noises were the same. These

Table 2. Simulation Results at the Different Values of l_ε with Noise

l_ε (μm)	0	10	20	30	40
a_0 (rad)	12.242	−60.381	−134.747	−208.636	−280.721
a_1 (rad·μm)	0.185	67.237	135.419	203.301	270.052
$z_s - z_o$ (μm)	−0.015	−5.351	−10.776	−16.178	−21.490
$z_p - z_o$ (μm)	0.002	−5.479	−10.630	−16.110	−21.596

Table 3. Differences in $z_s - z_o$ and $z_p - z_o$ between Tables 1 and 2

l_ε (μm)	0	10	20	30	40
$\Delta(z_s - z_o)$ (nm)	−15	29	−17	−39	29
$\Delta(z_p - z_o)$ (nm)	2	−1	3	3	−2

Table 4. Simulation Results for Different Noises at $l_\varepsilon = 40$ μm

$\varphi_n(z)$	a_0 (rad)	a_1 (rad · μm)	$z_s - z_o$ (μm)	$z_p - z_o$ (μm)
Noise I	−280.721	270.052	−21.490	−21.596
Noise II	−287.446	270.324	−21.512	−21.594
Noise III	−282.214	271.023	−21.567	−21.595

noises produced different values of a_0 and a_1. The difference in the values of $z_s - z_o$ among the 3 noises was less than 55 nm. On the other hand, the difference in the values of $z_p - z_o$ among the 3 noises is less than 2 nm. The conclusions obtained from Table 2 do not change for different noises, and the value z_p provides high repeatability in surface profile measurement.

4. EXPERIMENT

A WLSI was constructed as shown in Fig. 1. The light source of interferometer was a supercontinuum light source whose spectral range was 400–1200 nm. The object was a glass with a step of 3 μm width on the surface. The reference surface was a glass with a wedge angle, and it was regarded as one reflecting surface. The two optical fields on the object and reference surfaces were made with the two lenses of L2 and L3 with unity magnification on the camera. The inclination of the reference surface was adjusted so that the phase distribution of the interference pattern on the camera did not indicate a large inclination of the object surface, which was caused by the distribution of the distance difference l_ε as shown in Tables 1 and 2. A high-speed camera was used as the detector. Its pixel size was 20 × 20 μm, and the frame size was 640 × 480 pixels. The measurement points of 56 × 41 pixels with the interval of 200 μm were made by adding up the interference signals detected on one pixel in the region of 10 × 10 pixels. The measuring points were denoted by N_x and N_y, where N_x was from 1 to 56, and N_y was from 1 to 41. The reference surface was moved by the PZT at a constant velocity of about 80 μm/s, and the sampling interval Δz of the interference signal was 39.6 nm. The data number N of the detected signal was 1024, and the required interference signal was selected with a rectangular window whose data number was 240. The other data outside the window were zero values. Figure 9 shows the windowed interference signal detected at a measurement point of $N_x = 18$ and $N_y = 18$, and the distance difference l_ε at this measurement point was about 45 μm. The interference signal indicates that the object position was about −1.23 μm. Although l_ε was equal to 88 μm at a measurement point $N_x = 1$ and $N_y = 18$, the object position indicated in the interference signal was −1.35 μm. This fact means that the inclination of the surface profile caused by l_ε did not appear in the detected interference signal. Fourier transform was performed on the windowed

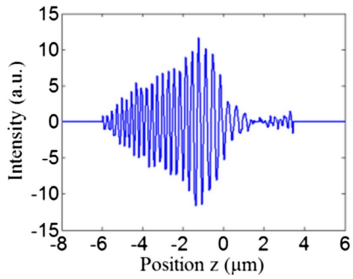

Fig. 9. Interference signal detected at measurement point of $N_x = 18$ and $N_y = 18$.

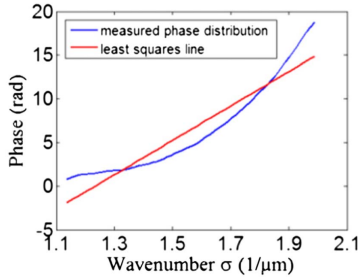

Fig. 10. Measured phase distribution of the interference in wavenumber domain and the least squares line of the distribution.

interference signal, where the interval of the wavenumber was $\Delta\sigma = 1/(2N\Delta z) = 0.0123\ \mu m^{-1}$. Figure 10 shows the phase of Fourier transform of the interference signal with blue color. The non-linear component of this phase distribution is almost similar to that in Fig. 7(b). The least squares line of the phase was shown by the red line. The values of a_0 and $a_1 - 4\pi z_o$ were −24.357 rad and 19.715 rad · μm, respectively. The measurement value z_s obtained from $a_1 - 4\pi z_o$ was −1.569 μm. Figure 11 shows the CVIS obtained by using the least squares line of the phase. The position z_a was −1.571 nm, and the measurement value z_p was −1.609 nm.

The signal processing to obtain the two measurement values of z_s and z_p was carried out for all of the measurement points to get surface profiles of the glass with the step shape. A surface profile obtained from the measured values of z_s is shown in Fig. 12, where the tilt and piston components were eliminated.

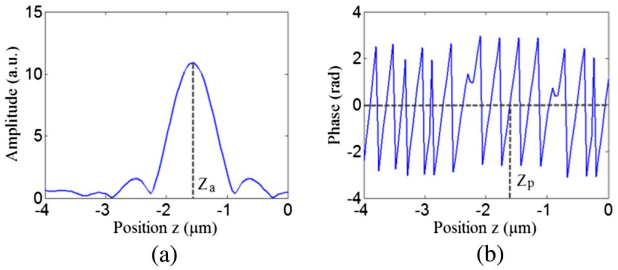

Fig. 11. Complex-valued interference signal of Fig. 9 obtained by using the least squares line of the phase shown in Fig. 10. $z_a = -1.583$ μm and $z_p = -1.609$ μm.

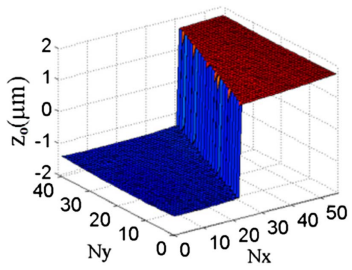

Fig. 12. Surface profile obtained from the measured values of z_s.

In order to show clearly the small variations in the surface profile, the surface profile on the left part in Fig. 12 is shown in Fig. 13. The magnitude of the small variations was less than 15 nm. Figure 14 shows the surface profile obtained from the measured values of z_p. The surface profile on the left part in Fig. 14 is shown in Fig. 15. The measured surface profile was very smooth, and the magnitude of the small variations was less than 4 nm. The repeatability was obtained by calculating a

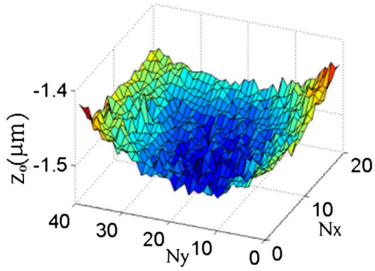

Fig. 13. Surface profile on the left part in Fig. 12.

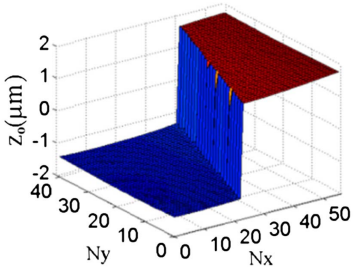

Fig. 14. Surface profile obtained from the measured values of z_p.

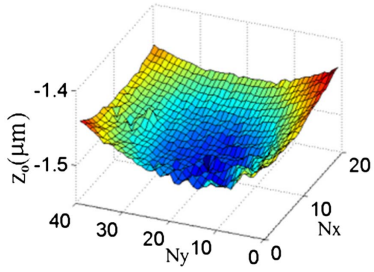

Fig. 15. Surface profile on the left side in Fig. 14.

root-mean-square value of the difference between two surface profiles measured in an interval of about 10 min. The repeatability was 1.3 nm in the measurement by z_p, while it was 13.3 nm in the measurement by z_s. The step width between $N_x = 34$ and $N_x = 37$ along $N_y = 28$ was 2.932 μm by the measured values of z_p. It was made clear that the measurement value z_p provides a more exact position of a measured reflecting surface than the measurement value z_s.

5. CONCLUSION

The simulation results agreed with the equations described in principle and made clear the characteristics of the proposed signal processing. The existence of the dispersion phase leads to the result that the values of a_1 and a_0 change linearly with increase in the distance difference l_e. This distribution of the value a_1 produces an inclination of a surface profile in the direction of the x axis along which the magnitude of the dispersion phase changes linearly. But this inclination of the surface profile can be eliminated by adjusting the inclination of the reference surface in experiments. The changes in the values of a_1 and a_0 caused by the random phase noise generate a large measurement error less than 15 nm in the value z_s, but the changes do not generate such a large measurement error in the value z_p. These characteristics of the proposed signal processing without using a measured dispersion phase lead to highly accurate measurement by the value z_p with an error less than 4 nm. In the future, it is required to investigate how the value of a_0 is made to compensate for the change in a_1, and also how the phase step of 2π appears in the value z_p.

Funding. National Natural Science Foundation of China (NSFC) (11674111, 61575070, 61605049); Natural Science Foundation of Fujian Province (2015I0005, 2017J01003).

REFERENCES

1. M. C. Park and S. W. Kim, "Direct quadratic polynomial fitting for fringe peak detection of white light scanning interferograms," Opt. Eng. **39**, 952–959 (2000).
2. P. de Groot, X. C. de Lega, J. Kramer, and M. Turzhitsky, "Determination of fringe order in white-light interference microscopy," Appl. Opt. **41**, 4571–4578 (2002).
3. A. Harasaki, J. Schmit, and J. C. Wyant, "Improved vertical-scanning interferometry," Appl. Opt. **39**, 2107–2115 (2000).
4. T. Pikálek, T. Fořt, and Z. Buchta, "Detection techniques in low-coherence interferometry and their impact on overall measurement accuracy," Appl. Opt. **53**, 8463–8470 (2014).
5. R. Hahn, J. Krauter, K. Körner, M. Gronle, and W. Osten, "Single-shot low coherence pointwise measuring interferometer with potential for in-line inspection," Meas. Sci. Technol. **28**, 025009 (2017).
6. P. de Groot and L. Deck, "Surface profiling by analysis of white-light interferograms in the spatial frequency domain," J. Mod. Opt. **42**, 389–401 (1995).
7. M. B. Sinclair, M. P. de Boer, and A. D. Corwin, "Long-working-distance incoherent-light interference microscope," Appl. Opt. **44**, 7714–7721 (2005).
8. S. Luo, O. Sasaki, Z. Chen, and J. Pu, "Utilization of complex-valued signals in a white-light scanning interferometer for accurate measurement of a surface profile," Appl. Opt. **56**, 4419–4425 (2017).